Science Advances
AAAS

advances.sciencemag.org/cgi/content/full/7/26/eabe6102/DC1

Supplementary Materials for

Strong links between Saharan dust fluxes, monsoon strength, and North Atlantic climate during the last 5000 years

Juncal A. Cruz, Frank McDermott, María J. Turrero, R. Lawrence Edwards, Javier Martín-Chivelet*

*Corresponding author. Email: martinch@ucm.es

Published 25 June 2021, *Sci. Adv.* **7**, eabe6102 (2021)
DOI: 10.1126/sciadv.abe6102

The PDF file includes:

Figs. S1 to S4
Tables S1 and S2
Legend for data file S1
References

Other Supplementary Material for this manuscript includes the following:

(available at advances.sciencemag.org/cgi/content/full/7/26/eabe6102/DC1)

Data file S1

Fig. S1.

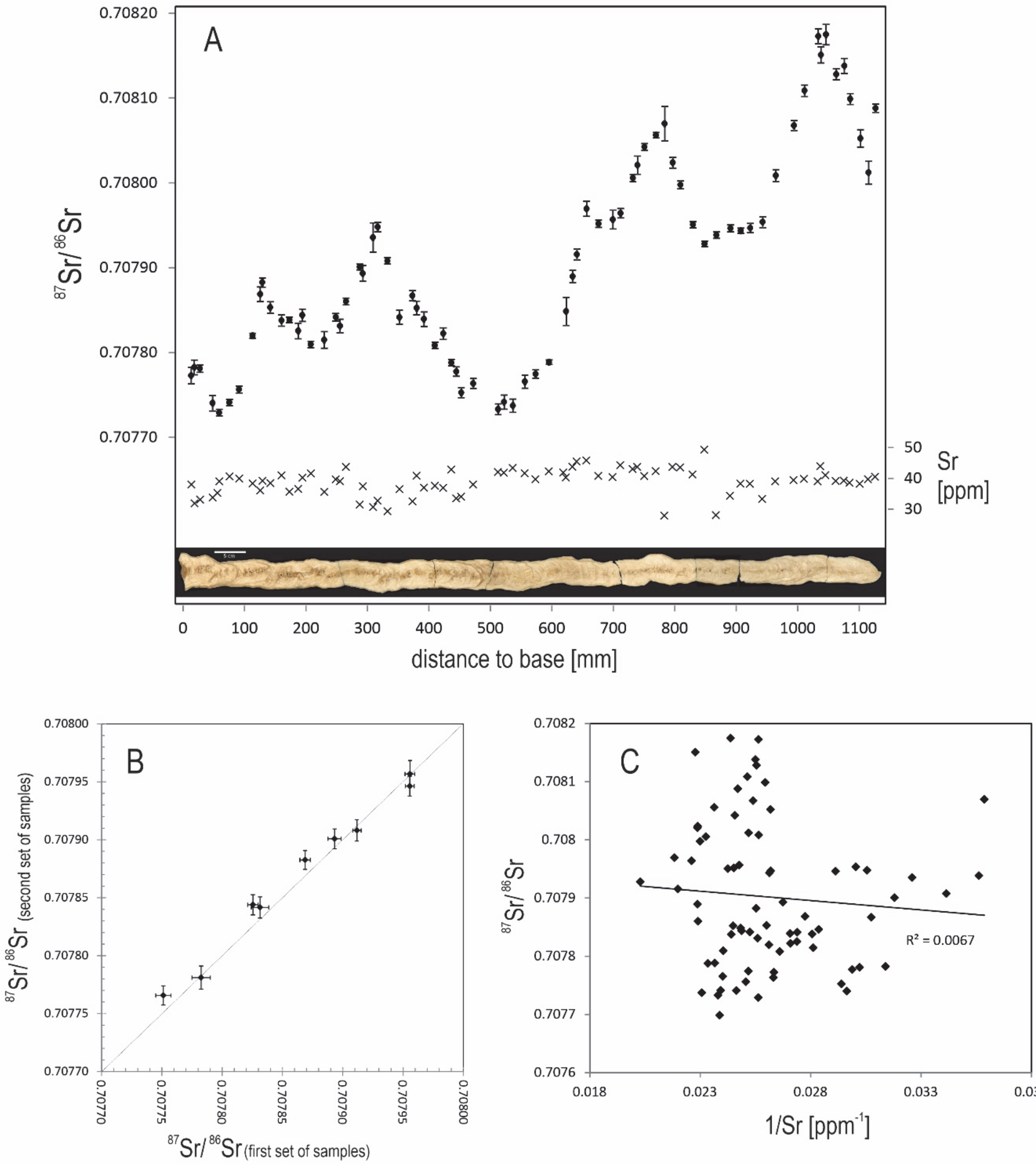

$^{87}Sr/^{86}Sr$ analytical results in Buda-100 stalagmite. A) $^{87}Sr/^{86}Sr$ ratios vs. stratigraphic position, represented by the vertical distance to the base of the stalagmite. The plot also includes the bulk strontium concentration of the same samples used for isotope measurements, which does not any clear trend nor variability pattern. **B)** Replicability of $^{87}Sr/^{86}Sr$ measurements checked by comparison of results of nine pairs of samples extracted from approximately the same stratigraphic levels. Linear correlation indicates excellent replicability. Observed minor deviations are related to the fact that each pair does not consists of two aliquots of one sample but to independently extracted samples. **C)** $^{87}Sr/^{86}Sr$ ratios *vs*. strontium concentration (1/Sr) showing lack of significant correlation between the two variables.

Fig. S2.

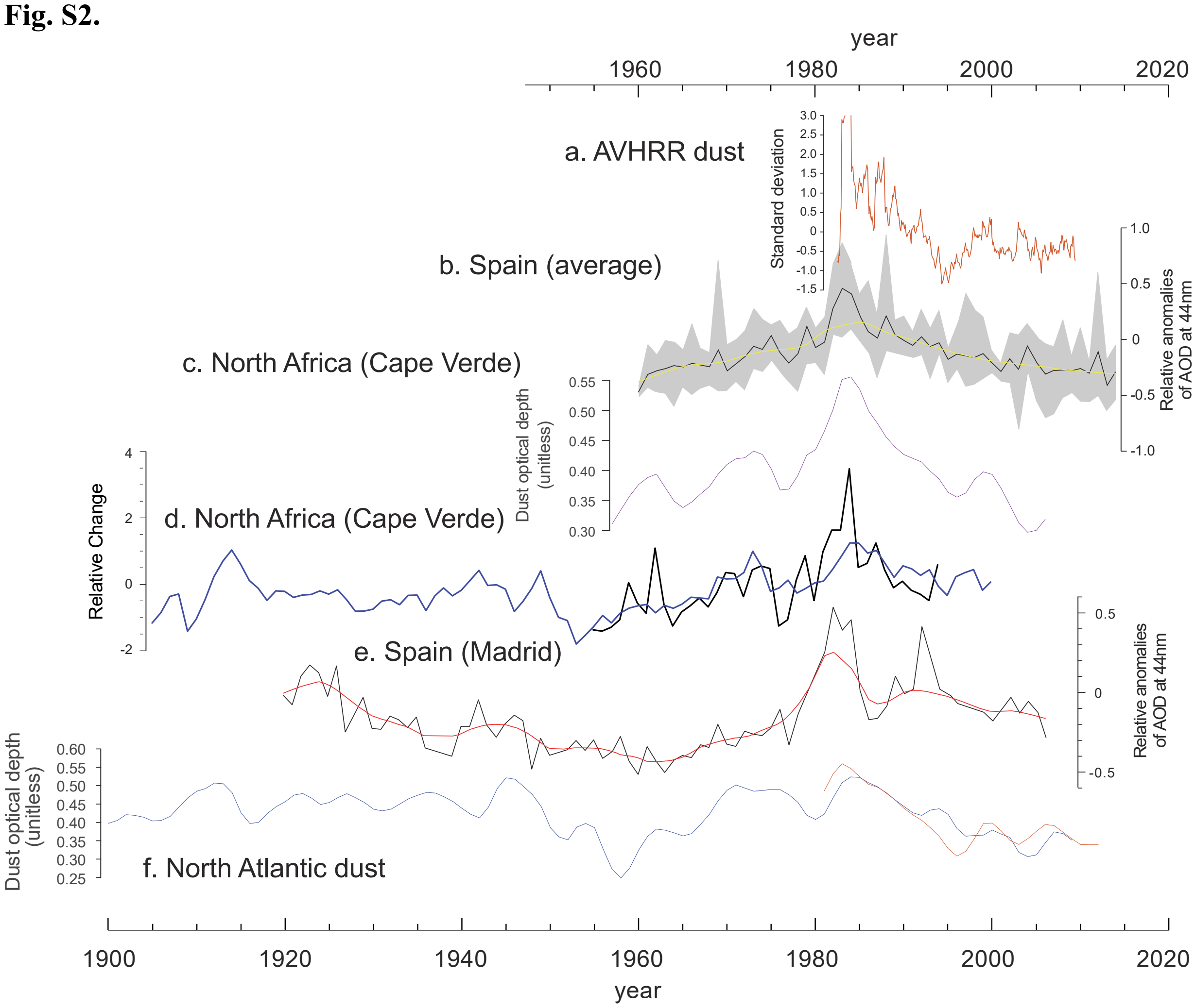

Inferred changes in dust influxes over Spain compared to NW Africa during the instrumental period. a) Dust optical depth averaged over the tropical North Atlantic from Advanced Very High Resolution Radiometer space-borne (AVHRR dust) (*81*), **b**) Mean relative anomalies of estimated AOD440 for summer (black line) for eight sites in Spain for 1961–2014 interval (yellow line: 11 years moving average; shaded area: maximum range for each year) (*82*), **c**) Hybrid satellite – coral reconstruction over the Cape Verde islands (15° N, 23.5° W) (*83*), **d**) Estimated relative dustiness for North Africa and North Atlantic. Cape Verde relative dustiness is shown in black, while North African dustiness (extrapolated using the Palmer Drought Severity Index-PDSI) is shown in blue (*84*); **e**) Relative anomalies of estimated AOD at 440 nm (black line) for Madrid (central Spain) in summer for 1920–2007 period (red line: 11-years moving average) (*82*). **f**) Estimates of North Atlantic dust (PC2 time series from the CIRES-20CR and ERA-I reanalyses) (*81*).

Fig. S3.

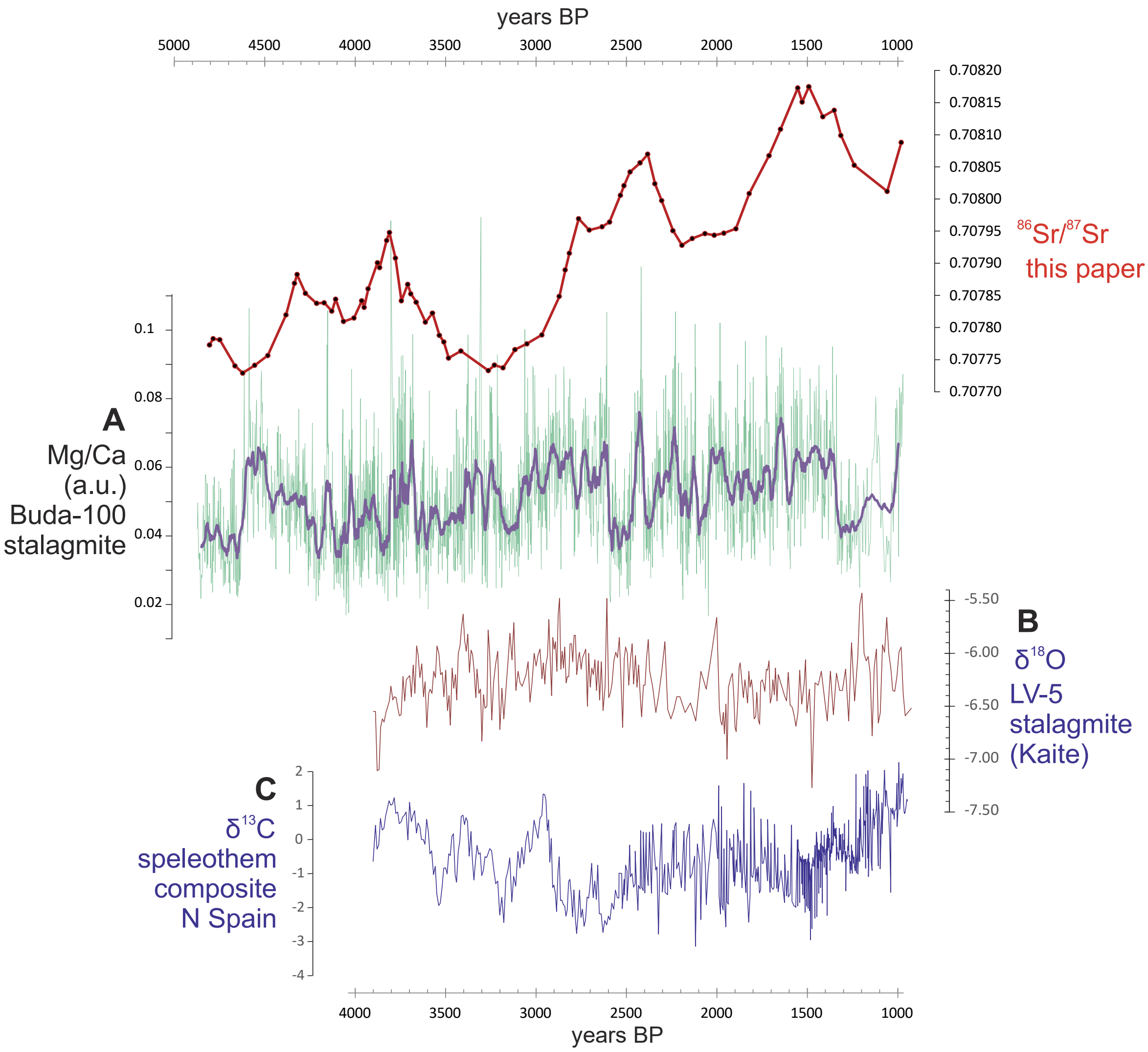

Paleoclimate records from Kaite Cave for the 5.0 to 1.0 ka BP interval, compared with the $^{86}Sr/^{87}Sr$ record. A) Mg/Ca series from stalagmite Buda-100, proxy of local hydroclimate, with higher values indicating drier conditions (*45*). Relative changes are however interpreted to be low. **B**) Calcite $\delta^{18}O$ of Kaite speleothem LV5 (*85*), with age model from (*86*). Changes in $\delta^{18}O$ have been interpreted to result from changes in precipitation amount, with higher values indicating lower amount (*87*), or alternatively from changes in seasonal rainfall patterns, with higher values indicating higher summer vs. winter rainfall (*44*). **C**) Calcite $\delta^{13}C$ composite curve from three speleothems from N Spain caves (including Kaite Cave) considered to reflect changes in surface temperature (*86*). The lack of correlation of these three records with the $^{86}Sr/^{87}Sr$ series, points in the same direction than the available instrumental series of dust influxes over Spain (Fig. S1) and the supra-regional correlations (Fig. 4): the dust changes detected in stalagmite Buda-100 are dominantly reflecting broad changes in dust source areas, being the influence of possible changes in regional dust transport or deposition subordinated.

Fig. S4.

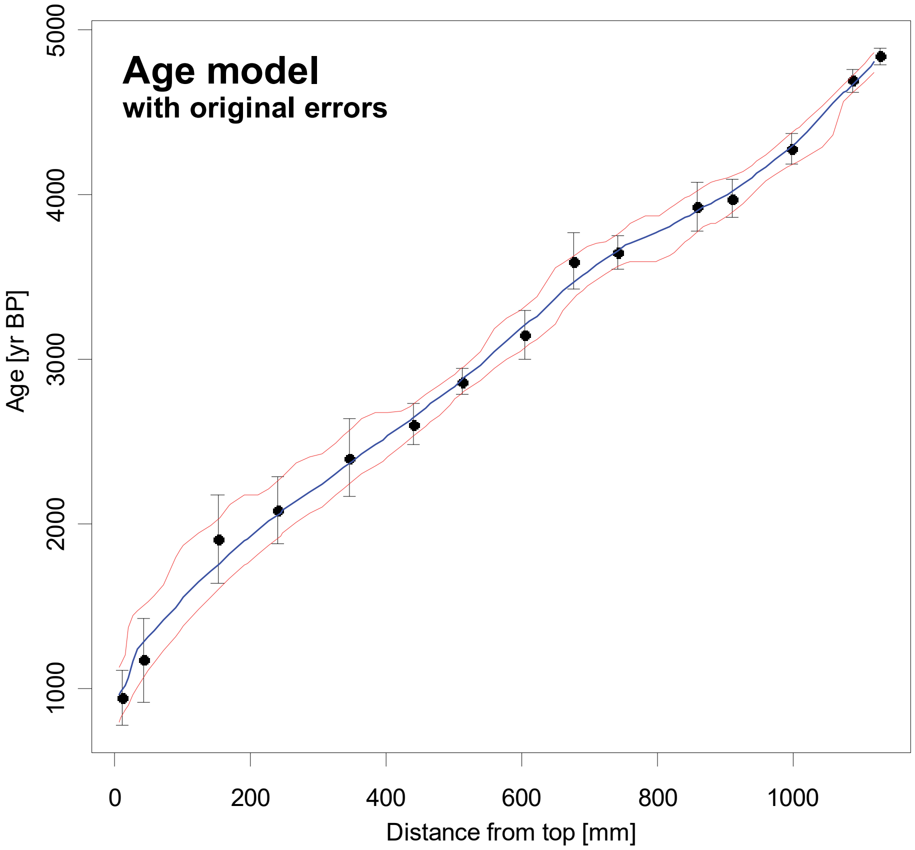

Age model for stalagmite Buda 100. Based in data from Table S2 and performed with StalAge software (*68*).

Table S1.

		$^{87}Sr/^{86}Sr$	Avg. Error	Number*	Std Dev
Present day speleothems	high growth	0.708386	± 2.1E-06	4	1.7E-06
	low growth	0.708295	± 2.0E-06	3	3.0E-05
Stalagmite	buda 100	0.707912	± 6.8E-06	89	1.2E-04
Drip waters	fast drip	0.708378	± 2.5E-06	4	3.7E-06
	slow drip	0.708301	± 2.8E-06	4	1.2E-05
Lithosol	soil leachate	0.708203	± 6.2E-06	4	1.5E-05
Host rock	host rock	0.707386	± 5.2E-06	8	3.3E-05
Sea spray	sea salt	0.709175	-	**	**
Rain	*clean* rain	0.709086	± 2.4E-06	4	5.8E-04
	dusty rain	0.720912	± 3.3E-06	5	1.3E-03
Saharan dust	Western North African PSA	0.7279	-	***	5.2E-03
	Central North African PSA	0.7186	-	***	5.3E-03
	Canary Islands accum.	0.725225	-	****	****

* Number of analyzed samples
**Sea salt isotope ratio according to (*70*).
***Isotope ratio for Western and Central North African preferential source dust areas (PSAs) according to (*20*)
****Isotope ratio for Canary Islands Saharan dust accumulations based in (*18*, *71*).

$^{87}Sr/^{86}Sr$ in Kaite Cave and speleothem strontium sources. The table includes averaged data for the sources of strontium (host rock, sea spray, Saharan dust) determining the $^{87}Sr/^{86}Sr$ ratio of the speleothems and included in the model for dust influx reconstruction. It also includes the isotopic ratios of present-day drip-waters and growing speleothems, necessary for model calibration, and the mean isotopic ratios measured in Buda-100 stalagmite. Additionally, to support the model and results, the $^{87}Sr/^{86}Sr$ of local rain and the poorly developed lithosol above the cave are also included. The lithosol mostly consists of imperfectly weathered fragments of the host rock and, to a much lesser extent, of fine sediment of aeolian origin. In order to simulate as closely as possible, the behavior of rainwater seeping through the soil, a soil leaching procedure was made to quantify loss of soluble substances and colloids. Since the soil cover is thin (lithosol), this method was used as analogue of water infiltration after a rain event. The procedure was as follow. 100 g of soil were ground and mixed in order to obtain a homogeneous sample. 4 soil fractions with a soil:water ratio 1:1 (2 x 10mg:10mL and 2 x 30mg:30mL) were stirred for 24 hours. Then, they were centrifuged, and the supernatant was filtered through 2 microns for analysis.

Table S2.

^{230}Th dating results for stalagmite Buda-100. The error is 2σ error.

Sample Ref.	^{238}U (ppb)	^{232}Th (ppt)	^{230}Th / ^{232}Th (atomic x10^{-6})	d^{234}U* (measured)	^{230}Th / ^{238}U (activity)	^{230}Th Age (yr) (uncorrected)	^{230}Th Age (yr BP) (corrected)	δ ^{234}U$_{Initial}$** (corrected)
BUDA-0.1	133.0±0.2	292±6	379±8	132.7±2.4	0.0504±0.0003	4959±30	**4841±50**	135±2
BUDA-0.2	103.7±0.2	331±7	252±5	125.5±2.9	0.0489±0.0004	4837±38	**4693±70**	127±3
BUDA 0.3	106.1±0.2	505±10	156±3	119.1±3.1	0.0449±0.0003	4466±34	**4281±94**	121±3
BUDA 0.4	105.3±0.2	636±13	115±2	116.7±3.1	0.0422±0.0003	4197±35	**3978±116**	118±3
BUDA 1.1	89.6±0.2	650±13	95±2	107.6±1.7	0.0417±0.0007	4181±68	**3929±151**	109±2
BUDA 1.2	98.7±0.2	498±10	126±3	110.9±3.4	0.0385±0.0004	3840±41	**3647±102**	112±3
BUDA2-3	108.5±0.2	986±20	73±2	119.5±3.2	0.0393±0.0004	3896±47	**3598±173**	121±3
BUDA 3.4	115.1±0.3	903±18	73±2	123.7±4.1	0.0346±0.0003	3409±35	**3145±148**	125±4
BUDA 3.5	166.2±0.2	636±13	131±3	113.3±1.7	0.0305±0.0003	3027±26	**2866±75**	114±2
BUDA 3.6	108.8±0.3	729±15	71±2	129.3±4.2	0.0290±0.0003	2840±35	**2607±127**	130±4
BUDA 4.7	83.9±0.2	1076±22	37±1	132.1±4.8	0.0286±0.0004	2790±45	**2400±237**	133±5
BUDA 5.8	119.6±0.2	1298±26	37±1	120.8±2.3	0.0247±0.0003	2425±34	**2082±202**	121±2
BUDA 6.9	125.3±0.3	1808±36	27±1	116.5±2.7	0.0238±0.0003	2344±27	**1907±268**	117±3
BUDA 7.10	114.1±0.2	1558±31	19±0	112.0±3.1	0.0161±0.0002	1592±25	**1173±254**	112±3
BUDA 7.11	139.3±0.3	1241±25	23±1	113.2±3.4	0.0126±0.0003	1240±27	**946±167**	114±3

*δ ^{234}U = ([^{234}U/^{238}U]$_{activity}$ – 1)x1000. ** δ^{234}U$_{initial}$ was calculated based on ^{230}Th age (T), i.e., δ^{234}U$_{initial}$ = δ^{234}U$_{measured}$ x e$^{\lambda 234 x T}$.
Corrected ^{230}Th ages assume the initial ^{230}Th/^{232}Th atomic ratio of 4.4 ± 2.2 x10^{-6}. Those are the values for a material at secular equilibrium, with the bulk earth ^{232}Th/^{238}U value of 3.8. The errors are arbitrarily assumed to be 50%.
BP stands for “Before Present” where the “Present” is defined as the year 1950 A.D.

^{230}Th dating results for stalagmite Buda-100. ^{230}Th age-dates were obtained using multicollector inductively coupled plasma–mass spectrometry (ICP-MS), following methods described in (*88*) and (*89*). The error is 2σ error.

Caption for Excel file F1 (abe6102_Excel_F1.xlsx)

This worksheet summarizes the mass-balance model used for calculating past dust deposition rates ($g \cdot m^{-2} \cdot y^{-1}$) in the study region (Kaite Cave, N Spain) from $^{87}Sr/^{86}Sr$ ratios measured in speleothem calcite. See Material and Methods section in the article for details.

REFERENCES AND NOTES

1. K. S. Carslaw, O. Boucher, D. V. Spracklen, G. W. Mann, J. G. L. Rae, S. Woodward, M. Kulmala, A review of natural aerosol interactions and feedbacks within the Earth system. *Atmos. Chem. Phys.* **10**, 1701–1737 (2010).

2. F. Solmon, M. Mallet, N. Elguindi, F. Giorgi, A. Zakey, A. Konaré, Dust aerosol impact on regional precipitation over western Africa, mechanisms and sensitivity to absorption properties. *Geophys. Res. Lett.* **35**, 1–6 (2008).

3. M. Kotsyfakis, S. G. Zarogiannis, E. Patelarou, The health impact of Saharan dust exposure. *Int. J. Occup. Med. Environ. Health* **32**, 749–760 (2019).

4. P. Ginoux, J. M. Prospero, T. E. Gill, N. C. Hsu, M. Zhao, Global-scale attribution of anthropogenic and natural dust sources and their emission rates based on MODIS Deep Blue aerosol products. *Rev. Geophys.* **50**, 1–36 (2012).

5. O. Boucher, D. Randall, P. Artaxo, C. Bretherton, G. Feingold, P. Forster, V.-M. Kerminen, Y. Kondo, H. Liao, U. Lohmann, P. Rasch, S. K. Satheesh, S. Sherwood, B. Stevens, X. Y. Zhang, in *Climate Change 2013 the Physical Science Basis: Working Group I Contribution to the Fifth Assessment Report of the Intergovernmental Panel on Climate Change*, T. F. Stocker, D. Qin, G.-K. Plattner, M. Tignor, S. K. Allen, J. Boschung, A. Nauels, Y. Xia, Eds. (Cambridge University Press, New York, 2013), pp. 571–658.

6. C. Wu, Z. Lin, X. Liu, The global dust cycle and uncertainty in CMIP5 (coupled model intercomparison project phase 5) models. *Atmos. Chem. Phys.* **20**, 10401–10425 (2020).

7. C. Wang, S. Dong, A. T. Evan, G. R. Foltz, S. K. Lee, Multidecadal covariability of north atlantic sea surface temperature, African dust, Sahel Rainfall, and Atlantic hurricanes. *J. Clim.* **25**, 5404–5415 (2012).

8. T. M. Shanahan, N. P. Mckay, K. A. Hughen, J. T. Overpeck, B. Otto-Bliesner, C. W. Heil, J. King, C. A. Scholz, J. Peck, The time-transgressive termination of the African humid period. *Nat. Geosci.* **8**, 140–144 (2015).

9. P. Sabatier, M. Nicolle, C. Piot, C. Colin, M. Debret, D. Swingedouw, Y. Perrette, M. C. Bellingery, B. Chazeau, A. L. Develle, M. Leblanc, C. Skonieczny, Y. Copard, J. L. Reyss, E. Malet, I. Jouffroy-Bapicot, M. Kelner, J. Poulenard, J. Didier, F. Arnaud, B. Vannière, Past African dust inputs in the western Mediterranean area controlled by the complex interaction between the Intertropical Convergence Zone, the North Atlantic Oscillation, and total solar irradiance. *Clim. Past* **16**, 283–298 (2020).

10. C. Zielhofer, H. von Suchodoletz, W. J. Fletcher, B. Schneider, E. Dietze, M. Schlegel, K. Schepanski, B. Weninger, S. Mischke, A. Mikdad, Millennial-scale fluctuations in Saharan dust supply across the decline of the African Humid Period. *Quat. Sci. Rev.* **171**, 119–135 (2017).

11. H. M. Clifford, N. E. Spaulding, A. V. Kurbatov, A. More, E. V. Korotkikh, S. B. Sneed, M. Handley, K. A. Maasch, C. P. Loveluck, J. Chaplin, M. McCormick, P. A. Mayewski, A 2000 year Saharan dust event proxy record from an ice core in the European Alps. *J. Geophys. Res. Atmos.* **124**, 12882–12900 (2019).

12. D. McGee, P. B. deMenocal, G. Winckler, J. B. W. Stuut, L. I. Bradtmiller, The magnitude, timing and abruptness of changes in North African dust deposition over the last 20,000 yr. *Earth Planet. Sci. Lett.* **371–372**, 163–176 (2013).

13. J. L. Middleton, S. Mukhopadhyay, C. H. Langmuir, J. F. McManus, P. J. Huybers, Millennial-scale variations in dustiness recorded in Mid-Atlantic sediments from 0 to 70 ka. *Earth Planet. Sci. Lett.* **482**, 12–22 (2018).

14. S. Mulitza, D. Heslop, D. Pittauerova, H. W. Fischer, I. Meyer, J. B. Stuut, M. Zabel, G. Mollenhauer, J. A. Collins, H. Kuhnert, M. Schulz, Increase in African dust flux at the onset of commercial agriculture in the Sahel region. *Nature* **466**, 226–228 (2010).

15. J. Adkins, P. deMenocal, G. Eshel, The "African humid period" and the record of marine upwelling from excess 230Th in Ocean Drilling Program Hole 658C. *Paleoceanography* **21**, PA4203 (2006).

16. P. Demenocal, J. Ortiz, T. Guilderson, J. Adkins, M. Sarnthein, L. Baker, M. Yarusinsky, Abrupt onset and termination of the African Humid Period: Rapid climate responses to gradual insolation forcing. *Quat. Sci. Rev.* **19**, 347–361 (2000).

17. S. Guerzoni, E. Molinaroli, R. Chester, Saharan dust inputs to the western Mediterranean Sea: Depositional. *Deep Res. II* **44**, 631–654 (1997).

18. D. Scheuvens, L. Schütz, K. Kandler, M. Ebert, S. Weinbruch, Bulk composition of northern African dust and its source sediments—A compilation. *Earth Sci. Rev.* **116**, 170–194 (2013).

19. P. Salvador, S. Alonso-Pérez, J. Pey, B. Artíñano, J. J. De Bustos, A. Alastuey, X. Querol, African dust outbreaks over the western Mediterranean Basin: 11-year characterization of atmospheric circulation patterns and dust source areas. *Atmos. Chem. Phys.* **14**, 6759–6775 (2014).

20. A. M. Jewell, N. Drake, A. J. Crocker, N. L. Bakker, T. Kunkelova, C. S. Bristow, M. J. Cooper, J. A. Milton, P. S. Breeze, P. A. Wilson, Three North African dust source areas and their geochemical fingerprint. *Earth Planet. Sci. Lett.* **554**, 116645 (2021).

21. S. Castillo, A. Alastuey, E. Cuevas, X. Querol, A. Avila, Quantifying dry and wet deposition fluxes in two regions of contrasting African influence: The NE Iberian Peninsula and the Canary Islands. *Atmosfera* **8**, 86 (2017).

22. I. J. Fairchild, P. C. Treble, Trace elements in speleothems as recorders of environmental change. *Quat. Sci. Rev.* **28**, 449–468 (2009).

23. A. Ayalon, M. Bar-Matthews, A. Kaufman, Petrography, strontium, barium and uranium concentrations, and strontium and uranium isotope ratios in speleothems as palaeoclimatic proxies: Soreq Cave, Israel. *The Holocene* **9**, 715–722 (1999).

24. A. Goede, M. McCulloch, F. McDermott, C. Hawkesworth, Aeolian contribution to strontium and strontium isotope variations in a tasmanian speleothem. *Chem. Geol.* **149**, 37–50 (1998).

25. J. L. Oster, I. P. Montañez, T. P. Guilderson, W. D. Sharp, J. L. Banner, Modeling speleothem δ13C variability in a central Sierra Nevada cave using 14C and 87Sr/86Sr. *Geochim. Cosmochim. Acta* **74**, 5228–5242 (2010).

26. A. Frumkin, M. Stein, The Sahara-East Mediterranean dust and climate connection revealed by strontium and uranium isotopes in a Jerusalem speleothem. *Earth Planet. Sci. Lett.* **217**, 451–464 (2004).

27. B. E. Wortham, C. I. Wong, L. C. R. Silva, D. McGee, I. P. Montañez, E. Troy Rasbury, K. M. Cooper, W. D. Sharp, J. J. G. Glessner, R. V. Santos, Assessing response of local moisture conditions in central Brazil to variability in regional monsoon intensity using speleothem 87Sr/86Sr values. *Earth Planet. Sci. Lett.* **463**, 310–322 (2017).

28. P. O. Hopcroft, P. J. Valdes, On the role of dust-climate feedbacks during the mid-Holocene. *Geophys. Res. Lett.* **46**, 1612–1621 (2019).

29. S. Egerer, M. Claussen, C. Reick, T. Stanelle, The link between marine sediment records and changes in Holocene Saharan landscape: Simulating the dust cycle. *Clim. Past* **12**, 1009–1027 (2016).

30. S. Albani, N. M. Mahowald, G. Winckler, R. F. Anderson, L. I. Bradtmiller, B. Delmonte, R. François, M. Goman, N. G. Heavens, P. P. Hesse, S. A. Hovan, S. G. Kang, K. E. Kohfeld, H. Lu, V. Maggi, J. A. Mason, P. A. Mayewski, D. McGee, X. Miao, B. L. Otto-Bliesner, A. T. Perry, A. Pourmand, H. M. Roberts, N. Rosenbloom, T. Stevens, J. Sun, Twelve thousand years of dust: The Holocene global dust cycle constrained by natural archives. *Clim. Past* **11**, 869–903 (2015).

31. R. H. Williams, D. McGee, C. W. Kinsley, D. A. Ridley, S. Hu, A. Fedorov, I. Tal, R. W. Murray, P. B. deMenocal, Glacial to Holocene changes in trans-Atlantic Saharan dust transport and dust-climate feedbacks. *Sci. Adv.* **2**, e1600445 (2016).

32. Y. H. Lee, K. Chen, P. J. Adams, Development of a global model of mineral dust aerosol microphysics. *Atmos. Chem. Phys.* **9**, 2441–2458 (2009).

33. P. DeMenocal, J. Ortiz, T. Guilderson, M. Sarnthein, Coherent high- and low-latitude climate variability during the holocene warm period. *Science* **288**, 2198–2202 (2000).

34. J. E. Tierney, F. S. R. Pausata, P. B. De Menocal, Rainfall regimes of the Green Sahara. *Sci. Adv.* **3**, e1601503 (2017).

35. J. A. Collins, M. Prange, T. Caley, L. Gimeno, B. Beckmann, S. Mulitza, C. Skonieczny, D. Roche, E. Schefuß, Rapid termination of the African Humid Period triggered by northern high-latitude cooling. *Nat. Commun.* **8**, 1372 (2017).

36. B. Damnati, Holocene lake records in the Northern Hemisphere of Africa. *J. Afr. Earth Sci.* **31**, 253–262 (2000).

37. C. Hély, A. M. Lézine, A. Ballouche, P. Cour, D. Duzer, P. Guinet, S. Jahns, J. Maley, A. M. Mercuri, A. Pons, J. C. Ritchie, U. Salzmann, E. Schulz, M. Van Campo, M. P. Waller, Holocene changes in African vegetation: Tradeoff between climate and water availability. *Clim. Past* **10**, 681–686 (2014).

38. M. C. Gatto, A. Zerboni, Holocene supra-regional environmental changes as trigger for major socio-cultural processes in northeastern Africa and the Sahara. *Afr. Archaeol. Rev*. **32**, 301–333 (2015).

39. S. Weldeab, D. W. Lea, R. R. Schneider, N. Andersen, Centennial scale climate instabilities in a wet early Holocene West African monsoon. *Geophys. Res. Lett.* **34**, L24702 (2007).

40. Y. Wang, H. Cheng, R. L. Edwards, Y. He, X. Kong, Z. An, J. Wu, M. J. Kelly, C. A. Dykoski, X. Li, The holocene Asian monsoon: Links to solar changes and North Atlantic climate. *Science* **308**, 854–857 (2005).

41. S. Weldeab, V. Menke, G. Schmiedl, The pace of East African monsoon evolution during the Holocene. *Geophys. Res. Lett.* **41**, 1724–1732 (2014).

42. G. H. Haug, K. A. Hughen, D. M. Sigman, L. C. Peterson, U. Röhl, Southward migration of the Intertropical Convergence Zone through the Holocene. *Science* **293**, 1304–1309 (2001).

43. C. C. Routson, N. P. McKay, D. S. Kaufman, M. P. Erb, H. Goosse, B. N. Shuman, J. R. Rodysill, T. Ault, Mid-latitude net precipitation decreased with Arctic warming during the Holocene. *Nature* **568**, 83–87 (2019).

44. L. M. Baldini, J. U. L. Baldini, F. McDermott, P. Arias, M. Cueto, I. J. Fairchild, D. L. Hoffmann, D. P. Mattey, W. Müller, D. C. Nita, R. Ontañón, C. Garciá-Moncó, D. A. Richards, North Iberian temperature and rainfall seasonality over the Younger Dryas and Holocene. *Quat. Sci. Rev.* **226**, 105998 (2019).

45. J. A. Cruz, M. J. Turrero, J. O. Cáceres, A. Marín-Roldán, A. I. Ortega, A. Garralón, L. Sánchez, P. Gómez, M. B. Muñoz-García, R. L. Edwards, J. Martín-Chivelet, Long-term hydrological changes in northern Iberia (4.9–0.9 ky BP) from speleothem Mg/Ca ratios and cave monitoring (Ojo Guareña Karst Complex, Spain). *Environ. Earth Sci.* **74**, 7741–7753 (2015).

46. A. Morley, Y. Rosenthal, P. DeMenocal, Ocean-atmosphere climate shift during the mid-to-late Holocene transition. *Earth Planet. Sci. Lett.* **388**, 18–26 (2014).

47. G. R. Foltz, M. J. McPhaden, Trends in Saharan dust and tropical Atlantic climate during 1980-2006. *Geophys. Res. Lett.* **35**, L20706 (2008).

48. B. Risebrobakken, E. Jansen, C. Andersson, E. Mjelde, K. Hevrøy, A high-resolution study of Holocene paleoclimatic and paleoceanographic changes in the Nordic Seas. *Paleoceanography* **18**, 1017 (2003).

49. M. Moros, K. Emeis, B. Risebrobakken, I. Snowball, A. Kuijpers, J. McManus, E. Jansen, Sea surface temperatures and ice rafting in the Holocene North Atlantic: Climate influences on northern Europe and Greenland. *Quat. Sci. Rev.* **23**, 2113–2126 (2004).

50. M. Moros, J. T. Andrews, D. D. Eberl, E. Jansen, Holocene history of drift ice in the northern North Atlantic: Evidence for different spatial and temporal modes. *Paleoceanography* **21**, PA2017 (2006).

51. T. L. Mjell, U. S. Ninnemann, T. Eldevik, H. K. F. Kleiven, Holocene multidecadal- to millennial-scale variations in Iceland-Scotland overflow and their relationship to climate. *Paleoceanography* **30**, 558–569 (2015).

52. D. W. Oppo, J. F. McManus, J. L. Cullen, Deepwater variability in the Holocene Epoch. *Nature* **422**, 277–78 (2003).

53. J. Schirrmacher, M. Weinelt, T. Blanz, N. Andersen, E. Salgueiro, R. R. Schneider, Multi-decadal atmospheric and marine climate variability in southern Iberia during the mid- to late-Holocene. *Clim. Past* **15**, 617–634 (2019).

54. H. Weiss, Global megadrought, societal collapse and resilience at 4.2-3.9 ka BP across the Mediterranean and west Asia. *Past Glob. Chang. Mag.* **24**, 62–63 (2016).

55. M. Bini, G. Zanchetta, A. Perşoiu, R. Cartier, A. Català, I. Cacho, J. R. Dean, F. Di Rita, R. N. Drysdale, M. Finnè, I. Isola, B. Jalali, F. Lirer, D. Magri, A. Masi, L. Marks, A. M. Mercuri, O. Peyron, L. Sadori, M. A. Sicre, F. Welc, C. Zielhofer, E. Brisset, The 4.2 ka BP Event in the Mediterranean region: An overview. *Clim. Past* **15**, 555–577 (2019).

56. B. van Geel, N. A. Bokovenko, N. D. Burova, K. V. Chugunov, V. A. Dergachev, V. G. Dirksen, M. Kulkova, A. Nagler, H. Parzinger, J. van der Plicht, S. S. Vasiliev, G. I. Zaitseva, Climate change and the expansion of the Scythian culture after 850 BC: A hypothesis. *J. Archaeol. Sci.* **31**, 1735–1742 (2004).

57. C. Martin-Puertas, K. Matthes, A. Brauer, R. Muscheler, F. Hansen, C. Petrick, A. Aldahan, G. Possnert, B. Van Geel, Regional atmospheric circulation shifts induced by a grand solar minimum. *Nat. Geosci.* **5**, 397–401 (2012).

58. S. Helama, P. D. Jones, K. R. Briffa, Dark Ages Cold Period: A literature review and directions for future research. *The Holocene* **27**, 1600–1606 (2017).

59. C. J. Wu, I. G. Usoskin, N. Krivova, G. A. Kovaltsov, M. Baroni, E. Bard, S. K. Solanki, Solar activity over nine millennia: A consistent multi-proxy reconstruction. *Astron. Astrophys.* **615**, 1–13 (2018).

60. H. Wanner, J. Beer, J. Bütikofer, T. J. Crowley, U. Cubasch, J. Flückiger, H. Goosse, M. Grosjean, F. Joos, J. O. Kaplan, M. Küttel, S. A. Müller, I. C. Prentice, O. Solomina, T. F. Stocker, P.

Tarasov, M. Wagner, M. Widmann, Mid- to Late Holocene climate change: An overview. *Quat. Sci. Rev.* **27**, 1791–1828 (2008).

61. G. Bond, B. Kromer, J. Beer, R. Muscheler, M. N. Evans, W. Showers, S. Hoffmann, R. Lotti-Bond, I. Hajdas, G. Bonani, Persistent solar influence on north atlantic climate during the Holocene. *Science* **294**, 2130–2136 (2001).

62. T. Kobashi, L. Menviel, A. Jeltsch-Thömmes, B. M. Vinther, J. E. Box, R. Muscheler, T. Nakaegawa, P. L. Pfister, M. Döring, M. Leuenberger, H. Wanner, A. Ohmura, Volcanic influence on centennial to millennial Holocene Greenland temperature change. *Sci. Rep.* **7**, 1441 (2017).

63. A. Klus, M. Prange, V. Varma, L. Bruno Tremblay, M. Schulz, Abrupt cold events in the North Atlantic Ocean in a transient Holocene simulation. *Clim. Past* **14**, 1165–1178 (2018).

64. S. Drijfhout, E. Gleeson, H. A. Dijkstra, V. Livina, Spontaneous abrupt climate change due to an atmospheric blocking-Sea-Ice-Ocean feedback in an unforced climate model simulation. *Proc. Natl. Acad. Sci. U.S.A.* **110**, 19713–19718 (2013).

65. J. F. Kok, D. S. Ward, N. M. Mahowald, A. T. Evan, Global and regional importance of the direct dust-climate feedback. *Nat. Commun.* **9**, 241 (2018).

66. A. A. Adebiyi, J. F. Kok, Climate models miss most of the coarse dust in the atmosphere. *Sci. Adv.* **6**, eaaz9507 (2020).

67. E. Philip Horwitz, R. Chiarizia, M. L. Dietz, A novel strontium-selective extraction chromatographic resin*. *Solvent Extr. Ion Exch.* **10**, 313–336 (1992).

68. D. Scholz, D. L. Hoffmann, StalAge - An algorithm designed for construction of speleothem age models. *Quat. Geochronol.* **6**, 369–382 (2011).

69. J. M. McArthur, R. J. Howarth, G. A. Shields, in *The Geologic Time Scale 2012*, F. M. Gradstein, J. G. Ogg, M. Schmitz, G. Ogg, Eds. (Elsevier B.V., 2012), pp. 127–144.

70. J. M. McArthur, Recent trends in strontium isotope stratigraphy. *Terra Nova* **6**, 331–358 (1994).

71. F. E. Grousset, M. Parra, A. Bory, P. Martinez, P. Bertrand, G. Shimmield, R. M. Ellam, Saharan wind regimes traced by the Sr-Nd isotopic composition of subtropical Atlantic sediments: Last Glacial Maximum vs today. *Quat. Sci. Rev.* **17**, 395–409 (1998).

72. N. M. Mahowald, A. R. Baker, G. Bergametti, N. Brooks, R. A. Duce, T. D. Jickells, N. Kubilay, J. M. Prospero, I. Tegen, Atmospheric global dust cycle and iron inputs to the ocean. *Glob. Biogeochem. Cycles* **19**, GB4025 (2005).

73. C. S. Zender, H. Bian, D. Newman, Mineral Dust Entrainment and Deposition (DEAD) model: Description and 1990s dust climatology. *J. Geophys. Res. D Atmos.* **108**, 4416 (2003).

74. P. Ginoux, M. Chin, I. Tegen, J. M. Prospero, B. Holben, O. Dubovik, S. J. Lin, Sources and distributions of dust aerosols simulated with the GOCART model. *J. Geophys. Res. Atmos.* **106**, 20255–20273 (2001).

75. A. Avila, L. Aguillaume, Monitorización y tendencias de la deposición de N en España, incluyendo polvo sahariano. *Ecosistemas* **26**, 16–24 (2017).

76. A. Avila, I. Queralt-Mitjans, M. Alarcón, Mineralogical composition of African dust delivered by red rains over northeastern Spain. *J. Geophys. Res. Atmos.* **102**, 21977–21996 (1997).

77. C. R. Lawrence, J. C. Neff, The contemporary physical and chemical flux of aeolian dust: A synthesis of direct measurements of dust deposition. *Chem. Geol.* **267**, 46–63 (2009).

78. N. M. Mahowald, J. F. Lamarque, X. X. Tie, E. Wolff, Sea-salt aerosol response to climate change: Last Glacial Maximum, preindustrial, and doubled carbon dioxide climates. *J. Geophys. Res. Atmos.* **111**, D05303 (2006).

79. A. Berger, M. F. Loutre, Insolation values for the climate of the last 10 million years. *Quat. Sci. Rev.* **10**, 297–317 (1991).

80. C. Waelbroeck, B. C. Lougheed, N. Vazquez Riveiros, L. Missiaen, J. Pedro, T. Dokken, I. Hajdas, L. Wacker, P. Abbott, J. P. Dumoulin, F. Thil, F. Eynaud, L. Rossignol, W. Fersi, A. L. Albuquerque, H. Arz, W. E. N. Austin, R. Came, A. E. Carlson, J. A. Collins, B. Dennielou, S.

Desprat, A. Dickson, M. Elliot, C. Farmer, J. Giraudeau, J. Gottschalk, J. Henderiks, K. Hughen, S. Jung, P. Knutz, S. Lebreiro, D. C. Lund, J. Lynch-Stieglitz, B. Malaizé, T. Marchitto, G. Martínez-Méndez, G. Mollenhauer, F. Naughton, S. Nave, D. Nürnberg, D. Oppo, V. Peck, F. J. C. Peeters, A. Penaud, R. da C. Portilho-Ramos, J. Repschläger, J. Roberts, C. Rühlemann, E. Salgueiro, M. F. Sanchez Goni, J. Schönfeld, P. Scussolini, L. C. Skinner, C. Skonieczny, D. Thornalley, S. Toucanne, D. Van Rooij, L. Vidal, A. H. L. Voelker, M. Wary, S. Weldeab, M. Ziegler, Consistently dated Atlantic sediment cores over the last 40 thousand years. *Sci. Data* **6**, 165 (2019).

81. A. T. Evan, C. Flamant, M. Gaetani, F. Guichard, The past, present and future of African dust. *Nature* **531**, 493–495 (2016).

82. A. Sanchez-Romero, A. Sanchez-Lorenzo, J. A. González, J. Calbó, Reconstruction of long-term aerosol optical depth series with sunshine duration records. *Geophys. Res. Lett.* **43**, 1296–1305 (2016).

83. A. T. Evan, S. Mukhopadhyay, African Dust over the Northern Tropical Atlantic: 1955–2008. *J. Appl. Meteorol. Climatol.* **49**, 2213–2229 (2010).

84. N. M. Mahowald, S. Kloster, S. Engelstaedter, J. K. Moore, S. Mukhopadhyay, J. R. McConnell, S. Albani, S. C. Doney, A. Bhattacharya, M. A. J. Curran, M. G. Flanner, F. M. Hoffman, D. M. Lawrence, K. Lindsay, P. A. Mayewski, J. Neff, D. Rothenberg, E. Thomas, P. E. Thornton, C. S. Zender, Observed 20th century desert dust variability: Impact on climate and biogeochemistry. *Atmos. Chem. Phys.* **10**, 10875–10893 (2010).

85. D. Domínguez-Villar, X. Wang, H. Cheng, J. Martín-Chivelet, R. L. Edwards, A high-resolution late Holocene speleothem record from Kaite Cave, northern Spain: δ18O variability and possible causes. *Quat. Int.* **187**, 40–51 (2008).

86. J. Martín-Chivelet, M. B. Muñoz-García, R. L. Edwards, M. J. Turrero, A. I. Ortega, Land surface temperature changes in Northern Iberia since 4000yrBP, based on δ13C of speleothems. *Glob. Planet. Chang.* **77**, 1–12 (2011).

87. D. Domínguez-Villar, X. Wang, K. Krklec, H. Cheng, R. L. Edwards, The control of the tropical North Atlantic on Holocene millennial climate oscillations. *Geology* **45**, 303–306 (2017).

88. R. L. Edwards, J. H. Chen, G. J. Wasserburg, ^{238}U-^{234}U-^{230}Th-^{232}Th systematics and the precise measurement of time over the past 500,000 years. *Earth Planet. Sci. Lett.* **81**, 175–192 (1987).

89. H. Cheng, R. L. Edwards, C. C. Shen, V. J. Polyak, Y. Asmerom, J. Woodhead, J. Hellstrom, Y. Wang, X. Kong, C. Spötl, X. Wang, E. Calvin Alexander, Improvements in ^{230}Th dating, ^{230}Th and ^{234}U half-life values, and U-Th isotopic measurements by multi-collector inductively coupled plasma mass spectrometry. *Earth Planet. Sci. Lett.* **371–372**, 82–91 (2013).